On-chip closed-loop optical circulation enabled by directional quantum squeezing

Qi-Zhong Hu(胡琦忠)[1], Lin-Peng You(游林鹏)[1], Pei Zhou(周培)[1], Lei Tang(唐磊)[1,*], Bang-Ping Hou(侯邦品)[1], Cong-Hua Yan(闫从华)[1]

[1]College of Physics and Electronic Engineering, Sichuan Normal University, Chengdu 610101, China

October 12, 2026

Abstract

Optical circulators are key components for integrated photonic information processing and quantum networks, yet realizing compact and magnet-free closed-loop circulation remains challenging. We propose an on-chip four-port optical circulator consisting of three evanescently coupled microring resonators, with directional quantum squeezing introduced into the central nonlinear resonator. The squeezing selectively enhances the effective inter-resonator coupling and renormalizes the resonance frequency for one propagation direction, while leaving the counterpropagating channel unaffected. This directional asymmetry breaks optical reciprocity and enables closed-loop circulation along $1 \to 2 \to 3 \to 4 \to 1$. At the optimal operating point, the circulator achieves a fidelity of approximately 0.99 and an average insertion loss of about 0.22 dB. In addition, pump-induced quantum noise can be suppressed by injecting a phase-matched broadband squeezed-vacuum field, allowing low-noise operation from the classical to the single-photon regime. The proposed scheme provides a compact, magnet-free, and chip-compatible route to closed-loop optical circulation, with potential applications in integrated optical routing and quantum photonic networks.

Keywords: optical nonreciprocity, closed-loop optical circulation, directional quantum squeezing, microring resonators

PACS: 42.50.-p, 42.50.Lc, 42.60.Da

1. Introduction

Optical isolators and circulators, enabled by optical nonreciprocity, are fundamental components for suppressing back-reflections and controlling directional information flow in photonic systems. A two-port optical isolator permits light transmission in one direction while blocking reverse propagation [1], whereas an optical circulator sequentially routes incident light among multiple ports [2–5]. In particular, a closed-loop optical circulator establishes a complete cyclic pathway in which each port serves as both an input and an output, following, for example, the routing sequence $1 \to 2 \to 3 \to 4 \to 1$. Compared with two-port isolation or open-ended directional routing, closed-loop

*Corresponding author. E-mail: tanglei@sicnu.edu.cn

circulation enables continuous multiport signal transfer and effective separation of incident and outgoing fields. These capabilities are important for classical photonic applications, including integrated communication circuits [6] and optical sensing [7,8]. In the quantum regime, optical circulators and closed-loop circulation can provide directional routing and port separation in quantum communication networks [9–12], facilitate nonreciprocal signal flow and backaction control in quantum sensing [13–15], and enable controlled transport of photonic quantum states in quantum-computing architectures [16–18]. Therefore, realizing compact and low-loss on-chip closed-loop optical circulation is of considerable importance for both classical and quantum photonic technologies.

Despite this demand, conventional optical circulators typically rely on magneto-optical effects to break time-reversal symmetry [19–21]. Although magneto-optical devices can provide robust nonreciprocal routing, the required magnetic materials and external bias fields impede miniaturization, monolithic integration, and compatibility with semiconductor and quantum-photonic platforms. To eliminate magnetic bias, magnet-free optical circulation and related nonreciprocal routing have been extensively investigated using spatiotemporal modulation [6,22–27], optical nonlinearities [28–30], optomechanical interactions [31–34], spin–momentum locking in chiral quantum-optical systems [35–37], susceptibility–momentum locking in warm atomic ensembles [38–41], electromagnetically induced transparency in cold atomic ensembles [42], and reservoir engineering [43]. Although these mechanisms have enabled optical nonreciprocity and various forms of directional routing, realizing a genuine on-chip closed-loop optical circulator remains substantially more demanding. Such a device must simultaneously maintain high transmission along every desired port-to-port channel, strongly suppress reverse transport, minimize and balance the insertion losses of different circulation paths, and preserve a consistent cyclic routing sequence among all ports. Meeting these requirements within a compact, stable, scalable, and magnet-free architecture remains a major challenge.

Directional quantum squeezing [44] provides a distinct route to overcoming these limitations. More generally, squeezed states generated by optical parametric processes [45] have become important quantum resources for both fundamental studies and practical applications [46–50]. Together with the recent progress in broadband squeezed-vacuum generation [51,52], these developments demonstrate the increasing experimental maturity and application potential of squeezed-light resources. Quantum squeezing can further be employed to engineer effective optical interactions by transforming a bare cavity mode into a squeezed mode [53–56]. When the squeezing process is made directional, the effective coupling strength and resonance frequency are selectively modified for one traveling-wave mode, while the counterpropagating mode remains unsqueezed. Consequently, opposite propagation directions experience distinct coupled-mode dynamics, providing a controllable mechanism for breaking optical reciprocity without magnetic fields. This principle has been employed to realize on-chip optical isolation and three-port quasicirculation in a two-resonator system [44]. However, the resulting routing path was not closed and therefore did not constitute a genuine closed-loop optical circulator. Extending directional quantum squeezing from isolation and open routing to complete multiport circulation thus requires a new resonator architecture and coordinated control of all desired transmission channels.

Building on this mechanism, we propose an on-chip four-port closed-loop optical circulator based on three evanescently coupled microring resonators and three adjacent waveguides. Directional quantum squeezing is introduced into the central nonlinear resonator. Signal fields injected from ports 1 and 3 in-

teract with the squeezed traveling-wave mode and experience squeezing-enhanced inter-resonator couplings together with a renormalized resonance frequency, whereas fields injected from ports 2 and 4 couple to the corresponding unsqueezed mode. The resulting contrast between the coupled-mode dynamics of the two propagation directions produces pronounced transmission asymmetry and enables the complete closed-loop circulation sequence $1 \to 2 \to 3 \to 4 \to 1$. Moreover, a phase-matched broadband squeezed-vacuum field suppresses the pump-induced quantum noise without altering the coherent squeezing-enhanced dynamics, allowing high-fidelity, low-loss, and strongly isolated circulation from the classical to the single-photon regime. The proposed scheme therefore provides a chip-compatible and magnet-free route to a genuine closed-loop optical circulator and offers a promising platform for integrated optical routing, nonreciprocal quantum interfaces, and scalable chiral photonic networks.

2. Systems and Models

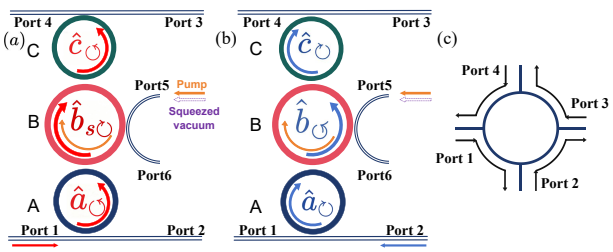


Fig. 1. Schematic of the proposed on-chip four-port closed-loop optical circulator enabled by directional quantum squeezing. Three whispering-gallery-mode microring resonators are evanescently coupled, with the central $\chi^{(2)}$ nonlinear resonator B driven through an auxiliary waveguide by a coherent pump field and a broadband squeezed-vacuum field. Owing to directional phase matching, quantum squeezing is selectively induced in the clockwise (CW) mode of resonator B. (a) Signal fields injected from ports 1 and 3 excite the counterclockwise (CCW) modes of resonators A and C, respectively, and couple to the CW squeezed mode $\hat{b}_{s\circlearrowleft}$ in resonator B. (b) Signal fields injected from ports 2 and 4 excite the CW modes of resonators A and C and couple to the unsqueezed CCW mode $\hat{b}_{\circlearrowleft}$ in resonator B. The resulting asymmetry between the squeezed and unsqueezed transport channels produces nonreciprocal photon transmission. (c) Functional representation of the four-port closed-loop circulator, which routes incident photons sequentially along $1 \to 2 \to 3 \to 4 \to 1$.

Figure 1 schematically illustrates the proposed on-chip optical circulator, which consists of three evanescently coupled whispering-gallery-mode (WGM) microring resonators and three adjacent optical waveguides. The resonators can be fabricated from high-quality $\chi^{(2)}$ nonlinear materials, such as lithium niobate or aluminum nitride, thereby supporting degenerate parametric nonlinear interactions. Resonators A and C are linearly coupled to the central nonlinear resonator B with coupling strengths J_1 and J_2, respectively. A continuous-wave coherent pump field with frequency ω_p, strength Ω_p, and phase θ_p is injected into resonator B through port 5. The pump selectively excites the clockwise (CW) pump mode $\hat{d}_{\circlearrowleft}$ and induces a directional squeezing interaction for the CW signal mode $\hat{b}_{\circlearrowleft}$. Owing to the directional phase-matching condition of the $\chi^{(2)}$ parametric process, only the CW signal mode is squeezed into the Bogoliubov mode $\hat{b}_{s\circlearrowleft}$, whereas the counterclockwise (CCW) mode $\hat{b}_{\circlearrowleft}$ remains unaffected. Moreover, resonators A and C are intentionally designed with slightly detuned resonance frequencies relative to resonator B, such that the pump field cannot resonantly excite parametric nonlinear processes in these two auxiliary resonators. Consequently, directional quantum squeezing occurs exclu-

sively in resonator B, allowing us to focus solely on the squeezing dynamics of the central resonator.

Next, we discuss the cases where the signal fields are injected from different ports and how the directional pump modulates the inter-resonator interactions. As shown in Fig. 1(a), when a signal field is injected from port 1, it excites the counterclockwise (CCW) mode $\hat{a}_{\circlearrowleft}$ in resonator A. Meanwhile, the coherent pump field injected into resonator B selectively drives the clockwise (CW) pump mode and induces degenerate parametric amplification in the same propagation direction. Owing to the directional phase-matching condition of the $\chi^{(2)}$ nonlinear process, the CW signal mode $\hat{b}_{\circlearrowright}$ in resonator B is squeezed into the Bogoliubov mode $\hat{b}_{s\circlearrowright}$. Consequently, the CCW mode $\hat{a}_{\circlearrowleft}$ in resonator A coherently couples to the squeezed mode $\hat{b}_{s\circlearrowright}$ with an enhanced coupling strength J_{s1}. The squeezed mode $\hat{b}_{s\circlearrowright}$ further couples to the CCW mode $\hat{c}_{\circlearrowleft}$ in resonator C with coupling strength J_{s2}, thereby forming a directional transport channel mediated by the squeezed mode.

In contrast, as shown in Fig. 1(b), when the signal field is injected from port 2, it excites the clockwise (CW) mode $\hat{a}_{\circlearrowright}$ in resonator A. In this case, the propagation direction of the signal mode is opposite to the squeezing-selective direction induced by the pump field in resonator B. Therefore, no squeezing interaction is established for the corresponding mode in resonator B. Instead, the mode $\hat{a}_{\circlearrowright}$ only couples to the unsqueezed mode $\hat{b}_{\circlearrowright}$ with the bare coupling strength J_1. As a result, the effective inter-resonator interactions for the port-1 and port-2 input cases become fundamentally different, leading to asymmetric mode interaction and nonreciprocal photon transport.

Similarly, signal fields injected from ports 3 and 4 exhibit transport dynamics analogous to those for inputs from ports 1 and 2, respectively. The port-3 input propagates through the squeezing-enhanced channel mediated by the squeezed mode in resonator B, whereas the port-4 input couples only to the unsqueezed mode through the bare-coupling channel. Together, these direction-dependent transport pathways establish a complete nonreciprocal routing loop and realize four-port closed-loop optical circulation, as illustrated in Fig. 1(c).

In the rotating frame with respect to the half pump frequency $\omega_p/2$, the Hamiltonians for the signal fields injected from ports 1 and 3 can be generally written as

$$\hat{H}_j = \hat{H}_0 + \hat{H}_{\text{pump}} + \hat{H}_{j,\text{in}} , \quad (j = 1, 3) , \tag{1}$$

where

$$\begin{aligned}\hat{H}_0/\hbar = {} & \Delta_p^a \hat{a}_{\circlearrowleft}^\dagger \hat{a}_{\circlearrowleft} + \Delta_p^b \hat{b}_{\circlearrowright}^\dagger \hat{b}_{\circlearrowright} + \Delta_p^c \hat{c}_{\circlearrowleft}^\dagger \hat{c}_{\circlearrowleft} \\ & + J_1 \left(\hat{a}_{\circlearrowleft}^\dagger \hat{b}_{\circlearrowright} + \hat{a}_{\circlearrowleft} \hat{b}_{\circlearrowright}^\dagger \right) + J_2 \left(\hat{b}_{\circlearrowright}^\dagger \hat{c}_{\circlearrowleft} + \hat{b}_{\circlearrowright} \hat{c}_{\circlearrowleft}^\dagger \right) .\end{aligned} \tag{2}$$

Here, $\hat{H}_0$ describes the free evolution of the three cavity modes and their coherent inter-resonator couplings. The detunings are defined as $\Delta_p^i = \omega_i - \omega_p/2$ $(i = a, b, c)$, where ω_a, ω_b, and ω_c denote the resonance frequencies of the signal modes in resonators A, B, and C, respectively. The parameters J_1 and J_2 denote the coherent coupling strengths between resonators A and B and between resonators B and C, respectively. The pump-induced parametric interaction is described by

$$\hat{H}_{\text{pump}}/\hbar = \frac{\Omega_p}{2} \left(\hat{b}_{\circlearrowright}^{\dagger 2} e^{-i\theta_p} + \hat{b}_{\circlearrowright}^2 e^{i\theta_p} \right) , \tag{3}$$

which represents a degenerate parametric down-conversion process, where one pump photon at frequency ω_p is converted into two signal photons at frequency $\omega_p/2$. The pump amplitude Ω_p is determined by the pump power and the effective nonlinear interaction strength in resonator B.

The input-driving Hamiltonians for the port-1 and port-3 input cases are respectively given by

$$\hat{H}_{1,\text{in}}/\hbar = i\sqrt{2\kappa_{\text{ex}}^a} \left(\hat{a}_{\circlearrowleft,\text{in}} \hat{a}_{\circlearrowleft}^\dagger e^{-i\Delta_{\text{in}} t} - \hat{a}_{\circlearrowleft,\text{in}}^\dagger \hat{a}_{\circlearrowleft} e^{i\Delta_{\text{in}} t} \right) , \tag{4a}$$

$$\hat{H}_{3,\text{in}}/\hbar = i\sqrt{2\kappa_{\text{ex}}^c} \left(\hat{c}_{\circlearrowleft,\text{in}} \hat{c}_{\circlearrowleft}^\dagger e^{-i\Delta_{\text{in}} t} - \hat{c}_{\circlearrowleft,\text{in}}^\dagger \hat{c}_{\circlearrowleft} e^{i\Delta_{\text{in}} t} \right) . \tag{4b}$$

Here, $\kappa_{\text{ex}}^{a(c)}$ denotes the external coupling rate between resonator A (C) and its corresponding waveguide. The

operators $\hat{a}_{\circlearrowleft,\mathrm{in}}$ and $\hat{c}_{\circlearrowleft,\mathrm{in}}$ describe the incident signal fields injected from ports 1 and 3, respectively. The detuning $\Delta_{\mathrm{in}} = \omega_{\mathrm{in}} - \omega_p/2$ denotes the detuning between the input signal and half the pump frequency. Although the signal fields enter from different ports, the propagation directions inside the three resonators remain identical for the port-1 and port-3 input cases. As a result, the two input configurations are governed by the same effective Hamiltonian and differ only in the input-driving term.

Applying the Bogoliubov squeezing transformation [53,54]

$$\hat{b}_{s\circlearrowleft} = u\hat{b}_{\circlearrowleft} + ve^{-i\theta_p}\hat{b}^{\dagger}_{\circlearrowleft} , \tag{5}$$

with $u = \cosh r_p$, $v = \sinh r_p$, and

$$r_p = \frac{1}{4}\ln\left(\frac{1+\beta}{1-\beta}\right) , \quad \beta = \frac{\Omega_p}{\Delta_p^b} , \tag{6}$$

the Hamiltonians $\hat{H}_1$ and $\hat{H}_3$ are transformed into the squeezed-mode frame. Under the rotating-wave approximation, the counter-rotating terms can be neglected in the regime $\Delta_p^a + \Delta_p^b\sqrt{1-\beta^2} \gg vJ_1$ and $\Delta_p^c + \Delta_p^b\sqrt{1-\beta^2} \gg vJ_2$. The effective Hamiltonians in the rotating frame of the input frequency Δ_{in} can be written as

$$\begin{aligned}\hat{H}_j^s/\hbar =& \Delta_a\hat{a}^{\dagger}_{\circlearrowleft}\hat{a}_{\circlearrowleft} + \Delta_b^s\hat{b}^{\dagger}_{s\circlearrowleft}\hat{b}_{s\circlearrowleft} + \Delta_c\hat{c}^{\dagger}_{\circlearrowleft}\hat{c}_{\circlearrowleft} \\ &+ J_{s1}\left(\hat{a}^{\dagger}_{\circlearrowleft}\hat{b}_{s\circlearrowleft} + \hat{a}_{\circlearrowleft}\hat{b}^{\dagger}_{s\circlearrowleft}\right) \\ &+ J_{s2}\left(\hat{c}^{\dagger}_{\circlearrowleft}\hat{b}_{s\circlearrowleft} + \hat{c}_{\circlearrowleft}\hat{b}^{\dagger}_{s\circlearrowleft}\right) \\ &+ \hat{H}'_{j,\mathrm{in}}, \quad (j = 1,3) ,\end{aligned} \tag{7}$$

where the squeezing-enhanced coupling strengths are given by

$$J_{s1} = uJ_1 , \qquad J_{s2} = uJ_2 . \tag{8}$$

The effective detuning of the squeezed mode in resonator B is

$$\Delta_p^{bs} = \Delta_p^b\sqrt{1-\beta^2} , \tag{9}$$

and $\Delta_a = \omega_a - \omega_{\mathrm{in}}$, $\Delta_b^s = \Delta_p^{bs} - \Delta_{\mathrm{in}}$, and $\Delta_c = \omega_c - \omega_{\mathrm{in}}$.

The input-driving Hamiltonians are

$$\hat{H}'_{1,\mathrm{in}}/\hbar = i\sqrt{2\kappa_{\mathrm{ex}}^a}\left(\hat{a}_{\circlearrowleft,\mathrm{in}}\hat{a}^{\dagger}_{\circlearrowleft} - \hat{a}^{\dagger}_{\circlearrowleft,\mathrm{in}}\hat{a}_{\circlearrowleft}\right) , \tag{10a}$$

$$\hat{H}'_{3,\mathrm{in}}/\hbar = i\sqrt{2\kappa_{\mathrm{ex}}^c}\left(\hat{c}_{\circlearrowleft,\mathrm{in}}\hat{c}^{\dagger}_{\circlearrowleft} - \hat{c}^{\dagger}_{\circlearrowleft,\mathrm{in}}\hat{c}_{\circlearrowleft}\right) . \tag{10b}$$

To characterize the transport properties of the squeezing-enhanced system, we first derive the quantum Langevin equations from the master equation. After applying the Bogoliubov transformation, the dynamics of the density operator $\hat{\rho}_j$ $(j = 1,3)$ are governed by

$$\begin{aligned}\frac{\mathrm{d}}{\mathrm{d}t}\hat{\rho}_j =& -i\left[\hat{H}_j^s, \hat{\rho}_j\right] + \mathcal{L}\left[\hat{L}_a\right]\hat{\rho}_j + \mathcal{L}\left[\hat{L}_{bs}\right]\hat{\rho}_j \\ &+ \mathcal{L}\left[\hat{L}_c\right]\hat{\rho}_j + \mathcal{L}_n\left[\hat{L}_{bs}\right]\hat{\rho}_j ,\end{aligned} \tag{11}$$

where the Lindblad superoperator is defined as $\mathcal{L}[\hat{o}]\hat{\rho}_j = 2\hat{o}\hat{\rho}_j\hat{o}^{\dagger} - \hat{\rho}_j\hat{o}^{\dagger}\hat{o} - \hat{o}^{\dagger}\hat{o}\hat{\rho}_j$. The dissipative processes are described by $\hat{L}_a = \sqrt{\kappa_a}\hat{a}_{\circlearrowleft}$, $\hat{L}_{bs} = \sqrt{\kappa_b}\hat{b}_{s\circlearrowleft}$, and $\hat{L}_c = \sqrt{\kappa_c}\hat{c}_{\circlearrowleft}$, where κ_a, κ_b, and κ_c denote the total decay rates of resonators A, B, and C, respectively. The additional term $\mathcal{L}_n[\hat{L}_{bs}]\hat{\rho}_j$ originates from the coherent parametric pump and represents the effective thermal and correlation noise associated with the squeezed mode $\hat{b}_{s\circlearrowleft}$ [53,54]. Such pump-induced noise degrades the coherence of single-photon transport and must be suppressed for quantum applications.

Following Refs. [44,53–55], a broadband squeezed-vacuum field [51,52] is injected into resonator B to eliminate the pump-induced noise. When the squeezed-vacuum field is mode matched to the coherent pump, namely $r_e = r_p$ and $\theta_e + \theta_p = \pm n\pi$ (n is an integer), the effective noise coefficients satisfy $\mathcal{L}_n[\hat{L}_{bs}]\hat{\rho}_j = 0$. Under this condition, all noise-correlation terms vanish and the master equation reduces to

$$\begin{aligned}\frac{\mathrm{d}}{\mathrm{d}t}\hat{\rho}_j^{\mathrm{sv}} =& -i\left[\hat{H}_j^s, \hat{\rho}_j^{\mathrm{sv}}\right] + \mathcal{L}\left[\hat{L}_a\right]\hat{\rho}_j^{\mathrm{sv}} + \mathcal{L}\left[\hat{L}_{bs}\right]\hat{\rho}_j^{\mathrm{sv}} \\ &+ \mathcal{L}\left[\hat{L}_c\right]\hat{\rho}_j^{\mathrm{sv}} .\end{aligned} \tag{12}$$

Therefore, the squeezed-vacuum field removes the pump-induced decoherence without modifying the coherent system dynamics, enabling robust single-photon nonreciprocal transport.

Based on the noise-free master equation, the steady-state transport properties can be obtained from the corresponding Langevin equations. For a signal

field injected from port 1, the input-output relations are given by [57]

$$\hat{a}_{\circlearrowleft,\mathrm{out}} = \hat{a}_{\circlearrowleft,\mathrm{in}} - \sqrt{2\kappa_{\mathrm{ex}}^{a}}\hat{a}_{\circlearrowleft} \ , \qquad \hat{c}_{\circlearrowleft,\mathrm{out}} = \sqrt{2\kappa_{\mathrm{ex}}^{c}}\hat{c}_{\circlearrowleft} \ . \tag{13}$$

The transmission coefficients from port 1 to ports 2 and 4 are defined as

$$T_{12} = \frac{\left\langle \hat{a}^{\dagger}_{\circlearrowleft,\mathrm{out}}\hat{a}_{\circlearrowleft,\mathrm{out}} \right\rangle}{\left\langle \hat{a}^{\dagger}_{\circlearrowleft,\mathrm{in}}\hat{a}_{\circlearrowleft,\mathrm{in}} \right\rangle} \ , \qquad T_{14} = \frac{\left\langle \hat{c}^{\dagger}_{\circlearrowleft,\mathrm{out}}\hat{c}_{\circlearrowleft,\mathrm{out}} \right\rangle}{\left\langle \hat{a}^{\dagger}_{\circlearrowleft,\mathrm{in}}\hat{a}_{\circlearrowleft,\mathrm{in}} \right\rangle} \ . \tag{14}$$

Solving the Langevin equations in the steady state yields

$$T_{12} = \frac{\left|\mathcal{G}_s - 2\kappa_{\mathrm{ex}}^{a}N_s\right|^2}{\left|\mathcal{G}_s\right|^2} \ , \qquad T_{14} = \frac{4\kappa_{\mathrm{ex}}^{a}\kappa_{\mathrm{ex}}^{c}J_{s1}^2J_{s2}^2}{\left|\mathcal{G}_s\right|^2} \ , \tag{15}$$

where $\mathcal{G}_s = (i\Delta_a + \kappa_a)\left[(i\Delta_b^s + \kappa_b)(i\Delta_c + \kappa_c) + J_{s2}^2\right] + J_{s1}^2(i\Delta_c + \kappa_c)$ and $N_s = (i\Delta_b^s + \kappa_b)(i\Delta_c + \kappa_c) + J_{s2}^2$.

Similarly, for a signal field injected from port 3,

$$\hat{a}_{\circlearrowleft,\mathrm{out}} = \sqrt{2\kappa_{\mathrm{ex}}^{a}}\hat{a}_{\circlearrowleft} \ , \qquad \hat{c}_{\circlearrowleft,\mathrm{out}} = \hat{c}_{\circlearrowleft,\mathrm{in}} - \sqrt{2\kappa_{\mathrm{ex}}^{c}}\hat{c}_{\circlearrowleft} \ , \tag{16}$$

and the transmission coefficients are defined as

$$T_{34} = \frac{\left\langle \hat{c}^{\dagger}_{\circlearrowleft,\mathrm{out}}\hat{c}_{\circlearrowleft,\mathrm{out}} \right\rangle}{\left\langle \hat{c}^{\dagger}_{\circlearrowleft,\mathrm{in}}\hat{c}_{\circlearrowleft,\mathrm{in}} \right\rangle} \ , \qquad T_{32} = \frac{\left\langle \hat{a}^{\dagger}_{\circlearrowleft,\mathrm{out}}\hat{a}_{\circlearrowleft,\mathrm{out}} \right\rangle}{\left\langle \hat{c}^{\dagger}_{\circlearrowleft,\mathrm{in}}\hat{c}_{\circlearrowleft,\mathrm{in}} \right\rangle} \ . \tag{17}$$

Signal fields injected from ports 1 and 3 experience identical propagation directions and squeezing-enhanced interactions inside the three resonators, and therefore exhibit the same transmission characteristics:

$$T_{34} = T_{12} \ , \qquad T_{32} = T_{14} \ . \tag{18}$$

For the port-2 and port-4 input cases, the system operates in the unsqueezed transport regime. In resonator B, the signal field excites the CCW mode $\hat{b}_{\circlearrowleft}$, whereas the pump field drives the CW mode. Since the signal and pump fields propagate in opposite directions, the directional phase-matching condition is not satisfied. Consequently, no degenerate parametric amplification occurs in resonator B, and the squeezing interaction is absent. The transport dynamics are therefore governed solely by the intrinsic inter-resonator couplings.

In the rotating frame of the input frequency ω_{in}, the Hamiltonians for the port-2 and port-4 input cases can be written in a unified form as

$$\begin{aligned}\hat{H}_j/\hbar = {} & \Delta_a\hat{a}^{\dagger}_{\circlearrowleft}\hat{a}_{\circlearrowleft} + \Delta_b\hat{b}^{\dagger}_{\circlearrowleft}\hat{b}_{\circlearrowleft} + \Delta_c\hat{c}^{\dagger}_{\circlearrowleft}\hat{c}_{\circlearrowleft} \\ & + J_1\left(\hat{b}^{\dagger}_{\circlearrowleft}\hat{a}_{\circlearrowleft} + \hat{a}^{\dagger}_{\circlearrowleft}\hat{b}_{\circlearrowleft}\right) + J_2\left(\hat{b}^{\dagger}_{\circlearrowleft}\hat{c}_{\circlearrowleft} + \hat{c}^{\dagger}_{\circlearrowleft}\hat{b}_{\circlearrowleft}\right) \\ & + \hat{H}_{j,\mathrm{in}} \ , \quad (j = 2, 4)\end{aligned} \tag{19}$$

where $\Delta_a = \omega_a - \omega_{\mathrm{in}}$, $\Delta_b = \omega_b - \omega_{\mathrm{in}}$, and $\Delta_c = \omega_c - \omega_{\mathrm{in}}$ denote the effective detunings of resonators A, B, and C, respectively. The input-driving Hamiltonians are respectively given by

$$\hat{H}_{2,\mathrm{in}}/\hbar = i\sqrt{2\kappa_{\mathrm{ex}}^{a}}\left(\hat{a}_{\circlearrowleft,\mathrm{in}}\hat{a}^{\dagger}_{\circlearrowleft} - \hat{a}^{\dagger}_{\circlearrowleft,\mathrm{in}}\hat{a}_{\circlearrowleft}\right) \ , \tag{20a}$$

$$\hat{H}_{4,\mathrm{in}}/\hbar = i\sqrt{2\kappa_{\mathrm{ex}}^{c}}\left(c_{\circlearrowleft,\mathrm{in}}\hat{c}^{\dagger}_{\circlearrowleft} - c^{\dagger}_{\circlearrowleft,\mathrm{in}}\hat{c}_{\circlearrowleft}\right) \ , \tag{20b}$$

where $\hat{a}_{\circlearrowleft,\mathrm{in}}$ and $\hat{c}_{\circlearrowleft,\mathrm{in}}$ denote the incident signal fields injected from ports 2 and 4, respectively.

Since no Bogoliubov transformation is involved in this propagation direction, only ordinary quantum fluctuations associated with the intrinsic and external dissipation channels remain. The dynamics of the density operator $\hat{\rho}_j$ $(j = 2, 4)$ are governed by

$$\begin{aligned}\frac{\mathrm{d}}{\mathrm{d}t}\hat{\rho}_j = {} & -i\left[\hat{H}_j, \hat{\rho}_j\right] + \mathcal{L}\left[\hat{L}_a\right]\hat{\rho}_j + \mathcal{L}\left[\hat{L}_b\right]\hat{\rho}_j \\ & + \mathcal{L}\left[\hat{L}_c\right]\hat{\rho}_j \ ,\end{aligned} \tag{21}$$

where $\hat{L}_a = \sqrt{\kappa_a}\hat{a}_{\circlearrowleft}$, $\hat{L}_b = \sqrt{\kappa_b}\hat{b}_{\circlearrowleft}$, $\hat{L}_c = \sqrt{\kappa_c}\hat{c}_{\circlearrowleft}$. For a signal field injected from port 2, the output fields at ports 1 and 3 are determined by the input-output relations [57]

$$\hat{a}_{\circlearrowleft,\mathrm{out}} = \hat{a}_{\circlearrowleft,\mathrm{in}} - \sqrt{2\kappa_{\mathrm{ex}}^{a}}\hat{a}_{\circlearrowleft} \ , \qquad \hat{c}_{\circlearrowleft,\mathrm{out}} = \sqrt{2\kappa_{\mathrm{ex}}^{c}}\hat{c}_{\circlearrowleft} \ . \tag{22}$$

Accordingly, the transmission coefficients from port 2 to ports 1 and 3 are defined as

$$T_{21} = \frac{\left\langle \hat{a}^{\dagger}_{\circlearrowleft,\mathrm{out}}\hat{a}_{\circlearrowleft,\mathrm{out}} \right\rangle}{\left\langle \hat{a}^{\dagger}_{\circlearrowleft,\mathrm{in}}\hat{a}_{\circlearrowleft,\mathrm{in}} \right\rangle} \ , \qquad T_{23} = \frac{\left\langle \hat{c}^{\dagger}_{\circlearrowleft,\mathrm{out}}\hat{c}_{\circlearrowleft,\mathrm{out}} \right\rangle}{\left\langle \hat{a}^{\dagger}_{\circlearrowleft,\mathrm{in}}\hat{a}_{\circlearrowleft,\mathrm{in}} \right\rangle} \ . \tag{23}$$

By solving the Langevin equations in the steady state, we obtain

$$T_{21} = \frac{\left|\mathcal{G}_0 - 2\kappa_{\mathrm{ex}}^{a}N_0\right|^2}{\left|\mathcal{G}_0\right|^2} \ , \qquad T_{23} = \frac{4\kappa_{\mathrm{ex}}^{a}\kappa_{\mathrm{ex}}^{c}J_1^2J_2^2}{\left|\mathcal{G}_0\right|^2} \ , \tag{24}$$

where $\mathcal{G}_0 = (i\Delta_a + \kappa_a)\left[(i\Delta_b + \kappa_b)(i\Delta_c + \kappa_c) + J_2^2\right] + J_1^2(i\Delta_c + \kappa_c)$, and $N_0 = (i\Delta_b + \kappa_b)(i\Delta_c + \kappa_c) + J_2^2$.

Similarly, for a signal field injected from port 4, the input-output relations become

$$\hat{a}_{\circlearrowleft,\mathrm{out}} = \sqrt{2\kappa_{\mathrm{ex}}^a}\hat{a}_{\circlearrowleft}\ , \qquad \hat{c}_{\circlearrowleft,\mathrm{out}} = \hat{c}_{\circlearrowleft,\mathrm{in}} - \sqrt{2\kappa_{\mathrm{ex}}^c}\hat{c}_{\circlearrowleft}\ , \tag{25}$$

The corresponding transmission coefficients are defined as

$$T_{41} = \frac{\left\langle \hat{a}^\dagger_{\circlearrowleft,\mathrm{out}}\hat{a}_{\circlearrowleft,\mathrm{out}}\right\rangle}{\left\langle \hat{c}^\dagger_{\circlearrowleft,\mathrm{in}}\hat{c}_{\circlearrowleft,\mathrm{in}}\right\rangle}\ , \qquad T_{43} = \frac{\left\langle \hat{c}^\dagger_{\circlearrowleft,\mathrm{out}}\hat{c}_{\circlearrowleft,\mathrm{out}}\right\rangle}{\left\langle \hat{c}^\dagger_{\circlearrowleft,\mathrm{in}}\hat{c}_{\circlearrowleft,\mathrm{in}}\right\rangle}\ . \tag{26}$$

Since the port-2 and port-4 input cases share the same effective Hamiltonian and differ only in the driving term, their steady-state transmission spectra satisfy

$$T_{43} = T_{21}\ , \qquad T_{41} = T_{23}\ . \tag{27}$$

3. Optical nonreciprocity and closed-loop circulation

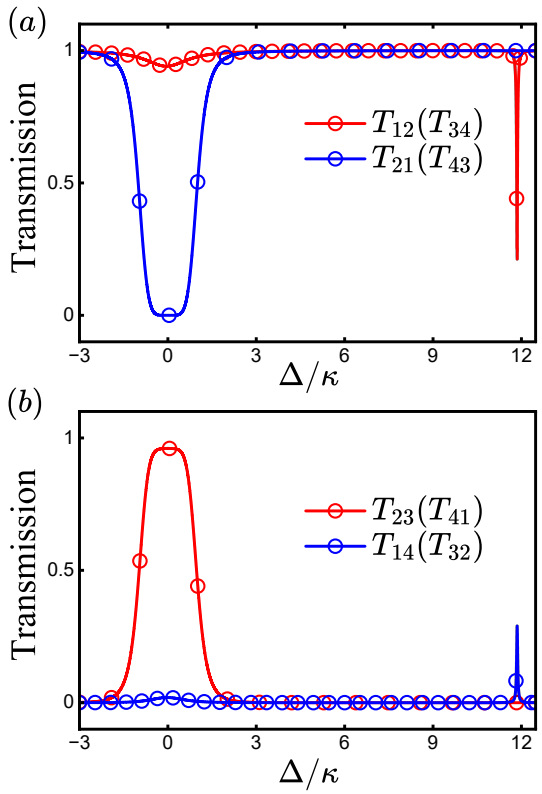


Fig. 2. Steady-state transmission spectra as functions of the detuning Δ/κ. (a) Transmissions T_{12} and T_{34} are shown by the red curve with red open circles, while the reverse transmissions T_{21} and T_{43} are shown by the blue curve with blue open circles. (b) Transmissions T_{23} and T_{41} are shown by the red curve with red open circles, while the reverse transmissions T_{32} and T_{14} are shown by the blue curve with blue open circles. Parameters: $J/\kappa = 0.7$, $\kappa_a = \kappa_c = \kappa$, $\kappa_b = 0.01\kappa$, $\kappa_{\mathrm{ex}}^a = \kappa_{\mathrm{ex}}^c = 0.99\kappa$, $\Delta_p^b/\kappa = 20$, $\Omega_p/\kappa = 18.2$, and $r_p \approx 0.76$.

According to Eqs. (15), (18), (24), and (27), the steady-state transmission coefficients T_{ij} can be obtained, where T_{ij} denotes the transmission from port i to port j. Figures 2(a) and 2(b) show the corresponding transmission spectra in the presence of directional quantum squeezing. The parameters are chosen as $\Delta_a = \Delta_b = \Delta_c = \Delta$, $J_1 = J_2 = J = 0.7\kappa$, $\kappa_a = \kappa_c = \kappa$, and $\kappa_{\mathrm{ex}}^a = \kappa_{\mathrm{ex}}^c = 0.99\kappa$. Here, resonators A and C are operated in the strongly overcoupled regime, such that their total decay rates are dominated by waveguide-coupling losses, while the corresponding intrinsic losses remain much smaller. For the signal mode in resonator B, the auxiliary waveguide is designed to provide a weak but finite external coupling through wavelength-selective coupling. Accordingly, we set the total decay rate of the signal mode in resonator B to $\kappa_b = 0.01\kappa$. The nonlinear resonator B is driven by a coherent pump with $\Omega_p/\kappa = 18.2$ and $\Delta_p^b/\kappa = 20$, yielding a squeezing parameter of $r_p \approx 0.76$.

As shown in the shaded region of Fig. 2, pronounced nonreciprocal transmission is obtained around resonance. At $\Delta = 0$, the desired transmission coefficients reach $T_{12} = T_{34} \approx 0.94$, while the corresponding reverse transmissions are suppressed to $T_{21} = T_{43} \approx 0$. For the other circulation paths, $T_{23} = T_{41} \approx 0.96$, whereas the reverse transmissions remain low, with $T_{32} = T_{14} \approx 0.02$. To quantify the nonreciprocity, we define the normalized isolation contrast as $\zeta = (T_{\mathrm{fw}} - T_{\mathrm{bw}})/(T_{\mathrm{fw}} + T_{\mathrm{bw}})$, where T_{fw} and T_{bw} denote the transmission coefficients along the desired circulation direction and the corresponding reverse direc-

tion, respectively. Specifically, $T_{\rm fw} = T_{12}(T_{34})$ and $T_{\rm bw} = T_{21}(T_{43})$ for one pair of circulation paths, while $T_{\rm fw} = T_{23}(T_{41})$ and $T_{\rm bw} = T_{32}(T_{14})$ for the other pair. The corresponding insertion loss is defined as $\mathscr{L} = -10\log_{10}(T_{\rm fw})$. At $\Delta = 0$, the normalized isolation contrasts are approximately 1 and 0.96, while the corresponding insertion losses are about 0.26 dB and 0.18 dB, respectively, demonstrating low-loss and high-isolation optical nonreciprocity.

The nonreciprocal response originates from the direction-dependent transport dynamics induced by directional quantum squeezing. For signal fields injected from ports 1 and 3, photons interact with the clockwise squeezed mode $\hat{b}_{s\circlearrowleft}$ in resonator B and therefore experience squeezing-modified inter-resonator interactions. By contrast, signal fields injected from ports 2 and 4 couple to the counterclockwise unsqueezed mode $\hat{b}_{\circlearrowright}$ and propagate through the bare-coupling configuration. As a result, the two propagation directions are governed by different effective Hamiltonians and exhibit markedly different port-to-port transmission characteristics. The resulting difference between the two propagation directions provides the physical basis for nonreciprocal transmission and closed-loop circulation.

Directional quantum squeezing modifies the squeezing-enhanced transport configuration through two complementary effects. First, it increases the effective inter-resonator coupling from J to J_s, as given by Eq. (8). As shown by the blue solid curve in Fig. 3(a), J_s/J increases monotonically with the squeezing parameter r_p. The enhanced coupling strengthens the hybridization among the three resonators and enlarges the normal-mode splitting of the squeezing-enhanced configuration. Consequently, its transmission spectrum is substantially modified relative to that of the bare-coupling configuration.

Second, the Bogoliubov transformation renormalizes the resonance frequency of the squeezed mode. As shown by the red dashed curve in Fig. 3(a), the effective detuning Δ_p^{bs} decreases continuously with increasing r_p, in accordance with Eqs. (6) and (9). This frequency renormalization shifts the resonance features of the squeezing-enhanced configuration and, under the chosen pump conditions, brings T_{12} and T_{34} close to their high-transmission condition around $\Delta = 0$, while T_{14} and T_{32} remain strongly suppressed. In contrast, the bare-coupling configuration favors the transmission channels T_{23} and T_{41}, whereas T_{21} and T_{43} are suppressed. These contrasting transmission characteristics therefore account for the port-selective spectral response observed in Fig. 2.

The squeezing strength can be continuously controlled through the pump parameter $\beta = \Omega_p/\Delta_p^b$. As shown in Fig. 3(b), r_p increases monotonically with β and rises rapidly as β approaches unity. Consequently, both the effective coupling enhancement and the squeezed-mode frequency renormalization can be tuned by adjusting the pump strength or pump detuning. This pump-controlled directional quantum squeezing enables the transmission characteristics of the squeezing-enhanced configuration to be properly matched with those of the bare-coupling configuration, resulting in high transmission along $1 \to 2$, $2 \to 3$, $3 \to 4$, and $4 \to 1$, while the competing port-to-port transmissions are strongly suppressed. These complementary routing characteristics establish the complete closed-loop circulation sequence $1 \to 2 \to 3 \to 4 \to 1$.

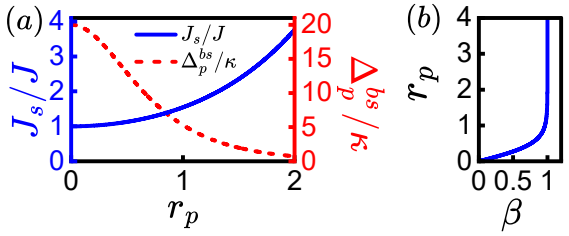


Fig. 3. (a) Effective inter-resonator coupling J_s/J (blue solid curve, left axis) and squeezed-mode detuning Δ_p^{bs}/κ (red dashed curve, right axis) as functions of the squeezing parameter r_p. Increasing r_p enhances the effective coupling while reducing the squeezed-mode detuning. (b) Squeezing parameter r_p as a function of the pump parameter $\beta = \Omega_p/\Delta_p^b$. The parameters are $\Delta_p^b/\kappa = 20$ and $\beta \in [0, 0.9999]$.

To quantitatively characterize the four-port circulator, we introduce the fidelity $\mathscr{F}$ and the average insertion loss $\bar{\mathscr{L}}$. The fidelity is defined as $\mathscr{F} = \mathrm{Tr}\left[\tilde{T}T_{\mathrm{id}}^{T}\right] / \mathrm{Tr}\left[T_{\mathrm{id}}T_{\mathrm{id}}^{T}\right]$ [38,44,58], where T_{id} denotes the transmission matrix of an ideal four-port circulator [59], whose nonzero elements satisfy $T_{12} = T_{23} = T_{34} = T_{41} = 1$. The normalized transmission matrix is given by $\tilde{T}_{ij} = T_{ij}/\varsigma_i$, with $\varsigma_i = \sum_j T_{ij}$. A fidelity approaching unity indicates that photons are routed to the desired output ports with minimal leakage into undesired channels. The average insertion loss is defined as $\bar{\mathscr{L}} = -10\log_{10}\left[(T_{12}+T_{23}+T_{34}+T_{41})/4\right]$, which characterizes the average signal attenuation along the desired circulation path.

Because the bare-coupling channels are unaffected by the directional squeezing, the circulator performance is mainly determined by the modification of the squeezed channels. Figure 4 shows $\mathscr{F}$ and $\bar{\mathscr{L}}$ as functions of r_p at $\Delta = 0$. In the absence of squeezing, the system is reciprocal and the fidelity starts from the reciprocal baseline $\mathscr{F} = 0.5$. As r_p increases, the fidelity rises rapidly and reaches a maximum value of approximately $\mathscr{F} = 0.99$ at $r_p \approx 0.76$. At the same operating point, the average insertion loss is minimized to approximately $\bar{\mathscr{L}} = 0.22$ dB, demonstrating high-fidelity and low-loss circulation. When r_p is increased beyond the optimal value, the squeezed-mode resonance moves away from the optimal spectral-matching condition. Consequently, the fidelity gradually decreases, while the average insertion loss increases. The optimal circulator performance therefore results from a balance between squeezing-enhanced coupling and resonance-frequency renormalization.

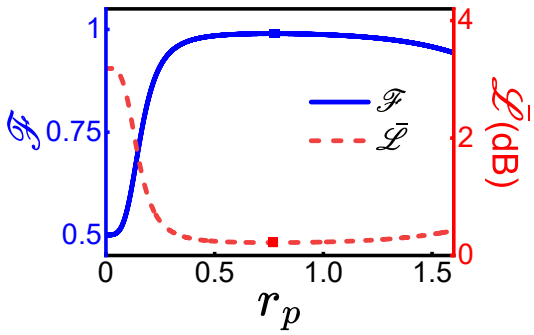


Fig. 4. Fidelity $\mathscr{F}$ (blue solid curve, left axis) and average insertion loss $\bar{\mathscr{L}}$ (red dashed curve, right axis) of the four-port optical circulator as functions of the squeezing parameter r_p at $\Delta = 0$. The square and circular markers denote the optimal operating point at $r_p \approx 0.76$, where the fidelity is maximized and the average insertion loss is minimized. The parameters are $J/\kappa = 0.7$, $\kappa_{\mathrm{ex}}^{a}/\kappa = \kappa_{\mathrm{ex}}^{c}/\kappa = 0.99$, and $\Delta_p^{b}/\kappa = 20$.

The transmission matrix at the optimal operating point is shown in Fig. 5. Its dominant elements closely reproduce the cyclic routing pattern of an ideal four-port circulator. Specifically, $T_{12} = T_{34} \approx 0.94$ and $T_{23} = T_{41} \approx 0.96$, indicating that photons injected into each port are predominantly directed to the next adjacent port along $1 \to 2 \to 3 \to 4 \to 1$. In contrast, the reverse transmission coefficients are strongly suppressed, with $T_{21} = T_{43} \approx 0$ and $T_{14} = T_{32} \approx 0.02$. These transmission characteristics confirm the desired closed-loop circulation at the optimal operating point. Using the same optimal parameter set, we further characterize the operational bandwidth in terms of the normalized isolation contrast defined above. For the two independent pairs of circulation paths, we denote the corresponding isolation contrasts by ζ_1, evaluated from T_{12} (T_{34}) and the corresponding reverse transmission T_{21} (T_{43}), and ζ_2, evaluated from T_{23} (T_{41}) and the reverse transmission T_{32} (T_{14}). We define the isolation-contrast bandwidth as the continuous frequency range over which both ζ_1 and ζ_2 exceed 0.95. Under this criterion, the calculated spectra yield a normalized operational bandwidth of $\Delta_{\mathrm{BW}}^{0.95}/\kappa = 1.08$. Within this bandwidth, the insertion losses of all desired circulation paths remain below 0.29 dB, indicating that the high isolation contrast is maintained together with efficient forward transmission over the entire operational

bandwidth.

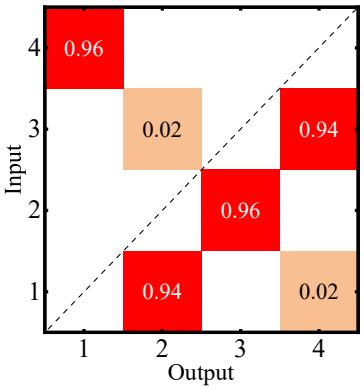


Fig. 5. Transmission matrix of the proposed four-port optical circulator at the optimal operating point $r_p = 0.76$ and $\Delta = 0$. The rows and columns denote the input and output ports, respectively, and the labeled elements give the corresponding transmission coefficients T_{ij}. Unlabeled white elements are negligibly small. Other parameters are the same as those in Fig. 2.

4. Discussion and conclusion

Our proposal can be implemented on an integrated platform consisting of three evanescently coupled microring resonators. Thin-film lithium niobate is a promising material platform because it combines strong second-order optical nonlinearity, high optical quality factors [60–62], and experimentally accessible single-photon nonlinear coupling strengths [63,64].

We consider a representative intrinsic quality factor of $Q_{\rm in} = 4\times10^6$ and a single-photon nonlinear coupling strength of $g/2\pi = 2.35$ MHz [63]. For a signal-mode resonance frequency of $\omega_i/2\pi = 193.4$ THz, the corresponding intrinsic field-decay rate is $\kappa^i_{\rm in} = \omega_i/(2Q_{\rm in}) \approx 2\pi \times 24.2$ MHz. The external coupling rates and inter-resonator coupling strengths can be engineered by controlling the resonator–waveguide and inter-resonator gaps [44]. For resonators A and C, taking $\kappa^a_{\rm ex} = \kappa^c_{\rm ex} = 2\pi \times 2.40$ GHz gives total decay rates $\kappa_a = \kappa_c = \kappa \approx 2\pi \times 2.42$ GHz. The coupling strengths adopted in our calculations, $J_1 = J_2 = 0.7\kappa$, then correspond to $J_1/2\pi = J_2/2\pi \approx 1.69$ GHz. With this value of κ, the normalized operational bandwidth $\Delta^{0.95}_{\rm BW}/\kappa = 1.08$, defined by the condition $\zeta_1, \zeta_2 \geq 0.95$, corresponds to a physical bandwidth of approximately 1.08×2.42 GHz ≈ 2.61 GHz. These values indicate that the coupling, decay, and operational-bandwidth parameters considered in our theoretical model are compatible with gap-engineered integrated microring structures. In practice, fabrication-induced variations in the resonator–resonator and resonator–waveguide gaps can lead to deviations of J_1, J_2, $\kappa^a_{\rm ex}$, and $\kappa^c_{\rm ex}$ from their nominal values, thereby introducing imbalance among the different circulation paths. Such variations can be reduced through accurate lithographic control and device calibration. In addition, residual resonance-frequency mismatch can be compensated by thermo-optic or electro-optic tuning, while the squeezing-enhanced interaction can be further optimized by adjusting the pump strength and detuning. These tuning degrees of freedom provide practical flexibility for approaching the desired operating condition after fabrication.

Based on these device parameters, the pump amplitude $\Omega_p = 18.2\kappa$ corresponds to $\Omega_p/2\pi \approx 44.0$ GHz. For $\Delta^b_p = 20\kappa$, the pump detuning is $\Delta^b_p/2\pi \approx 48.4$ GHz, and the ratio $\beta = \Omega_p/\Delta^b_p = 0.91$ yields the squeezing parameter $r_p \approx 0.76$. From $\Delta^b_p = \omega_b - \omega_p/2$, a signal-mode resonance at $\omega_b/2\pi = 193.4$ THz requires a pump frequency of approximately $\omega_p/2\pi = 386.70$ THz. The corresponding pump power can be estimated from $P_p = \hbar\omega_p\kappa_p^2\Omega_p^2/(16\pi g^2\kappa^p_{\rm ex})$, where κ_p and $\kappa^p_{\rm ex}$ denote the total and external decay rates of the pump mode in resonator B, respectively [44]. For an order-of-magnitude estimate, taking $\kappa_p = \kappa$ and $\kappa^p_{\rm ex} = \kappa^a_{\rm ex} = \kappa^c_{\rm ex}$ gives $P_p \approx 27.5$ mW. This moderate pump requirement, together with the experimentally accessible quality factors, nonlinear coupling strength, and gap-controlled coupling rates, supports the feasibility of implementing the proposed circulator on a thin-film lithium-niobate platform.

Although the above feasibility analysis focuses on a $\chi^{(2)}$ thin-film lithium-niobate platform, the underly-

ing mechanism can, in principle, be extended to $\chi^{(3)}$ nonlinear systems. In a Kerr microresonator, four-wave mixing driven below the parametric-oscillation threshold can generate spontaneous pair squeezing and provide the effective squeezing interaction required in our scheme [65]. Related third-order nonlinear quantum photonic processes have also been demonstrated in silicon [66] and AlGaAs-on-insulator microresonators [67]. These results suggest that the proposed directional-squeezing mechanism may be generalized to Si, SiN, and AlGaAsOI platforms, provided that the phase-matching and propagation conditions are appropriately engineered.

It is also useful to place the present scheme in the context of other magnet-free approaches to optical circulation. Spatiotemporal modulation provides flexible control of nonreciprocal transport, but typically requires high-speed external modulation and additional driving circuitry. Conventional nonlinear optical schemes can avoid magnetic bias, although their operation may be restricted by intensity dependence and dynamic-reciprocity considerations. Optomechanical approaches exploit mechanically mediated interactions, with their performance linked to the control of mechanical dissipation and thermal fluctuations, whereas reservoir-engineering schemes rely on carefully tailored coherent and dissipative couplings. Chiral light–matter interactions and atomic-ensemble schemes provide alternative mechanisms for directional transport, but generally require specific emitter–field coupling configurations or atomic media. In contrast, our scheme realizes genuine four-port closed-loop circulation in a compact all-optical resonator architecture through directional quantum squeezing, without magnetic bias or explicit temporal modulation. Moreover, the pump-induced quantum noise can be suppressed by a phase-matched squeezed-vacuum reservoir, enabling low-loss circulation from the classical regime toward weak-light and single-photon operation.

In conclusion, we have proposed an on-chip four-port optical circulator composed of three evanescently coupled microring resonators, in which directional quantum squeezing is introduced into the central nonlinear resonator. The direction-selective squeezing simultaneously enhances the effective inter-resonator coupling and renormalizes the squeezed-mode resonance frequency. This mechanism breaks optical reciprocity without magnetic fields or dynamic modulation and enables genuine closed-loop circulation along $1 \to 2 \to 3 \to 4 \to 1$, rather than the open routing supported by a three-port quasicirculator [44]. By applying a phase-matched broadband squeezed-vacuum field, the pump-induced quantum noise can be suppressed while preserving the squeezing-enhanced coherent dynamics, allowing high-fidelity and low-loss circulation in both the classical and single-photon regimes. The proposed scheme is compatible with integrated $\chi^{(2)}$ photonic platforms, particularly thin-film lithium niobate, and offers a promising route toward compact optical circulators, nonreciprocal quantum routers, and integrated quantum-information-processing networks. Moreover, the underlying directional-squeezing mechanism can be extended to larger coupled-resonator architectures, providing opportunities for reconfigurable closed-loop chiral transport and scalable nonreciprocal photonic circuits.

Acknowledgements

This work is supported by the National Natural Science Foundation of China (Grants No. 12305023), Sichuan Science and Technology Program (Grants No. 2024NSFSC1353).

References

[1] Jalas D, Petrov A, Eich M, Freude W, Fan S, Yu Z, Baets R, Popović M, Melloni A, Joannopoulos J D, Vanwolleghem M, Doerr C R and Renner H 2013 *Nat. Photonics* **7** 579–582 URL https://doi.org/10.1038/nphoton.2013.185

[2] Potton R J 2004 *Rep. Prog. Phys.* **67** 717 URL https://doi.org/10.1088/0034-4885/67/5/R03

[3] Huang D, Pintus P, Zhang C, Morton P, Shoji Y, Mizumoto T and Bowers J E 2017 *Optica* **4** 23–30 URL https://doi.org/10.1364/OPTICA.4.000023

[4] Caloz C, Alù A, Tretyakov S, Sounas D, Achouri K and Deck-Léger Z L 2018 *Phys. Rev. Appl.* **10**(4) 047001 URL https://doi.org/10.1103/PhysRevApplied.10.047001

[5] Asadchy V S, Mirmoosa M S, Díaz-Rubio A, Fan S and Tretyakov S A 2020 *Proc. IEEE* **108** 1684–1727 URL https://doi.org/10.1109/JPROC.2020.3012381

[6] Reiskarimian N and Krishnaswamy H 2016 *Nat. Commun.* **7** 11217 URL https://doi.org/10.1038/ncomms11217

[7] Suh M G and Vahala K J 2018 *Science* **359** 884–887 URL https://doi.org/10.1126/science.aao1968

[8] Lai Y H, Suh M G, Lu Y K, Shen B, Yang Q F, Wang H, Li J, Lee S H, Yang K Y and Vahala K 2020 *Nat. Photonics* **14** 345–349 URL https://doi.org/10.1038/s41566-020-0588-y

[9] Cirac J I, Zoller P, Kimble H J and Mabuchi H 1997 *Phys. Rev. Lett.* **78**(16) 3221–3224 URL https://doi.org/10.1103/PhysRevLett.78.3221

[10] Kimble H J 2008 *Nature* **453** 1023–1030 URL https://doi.org/10.1038/nature07127

[11] Wallucks A, Marinković I, Hensen B, Stockill R and Gröblacher S 2020 *Nat. Phys.* **16** 772–777 URL https://doi.org/10.1038/s41567-020-0891-z

[12] Chen Y A, Zhang Q, Chen T Y, Cai W Q, Liao S K, Zhang J, Chen K, Yin J, Ren J G, Chen Z, Han S L, Yu Q, Liang K, Zhou F, Yuan X, Zhao M S, Wang T Y, Jiang X, Zhang L and Liu W Y e a 2021 *Nature* **589** 214–219 URL https://doi.org/10.1038/s41586-020-03093-8

[13] Lupaşcu A, Saito S, Picot T, De Groot P C, Harmans C J P M and Mooij J E 2007 *Nat. Phys.* **3** 119–123 URL https://doi.org/10.1038/nphys509

[14] Palacios-Laloy A, Mallet F, Nguyen F, Bertet P, Vion D, Esteve D and Korotkov A N 2010 *Nat. Phys.* **6** 442–447 URL https://doi.org/10.1038/nphys1641

[15] Sathyamoorthy S R, Tornberg L, Kockum A F, Baragiola B Q, Combes J, Wilson C M, Stace T M and Johansson G 2014 *Phys. Rev. Lett.* **112**(9) 093601 URL https://doi.org/10.1103/PhysRevLett.112.093601

[16] Hacker B, Welte S, Rempe G and Ritter S 2016 *Nature* **536** 193–196 URL https://doi.org/10.1038/nature18592

[17] Lescanne R, Villiers M, Peronnin T, Sarlette A, Delbecq M, Huard B, Kontos T, Mirrahimi M and Leghtas Z 2020 *Nat. Phys.* **16** 509–513 URL https://doi.org/10.1038/s41567-020-0824-x

[18] Lecocq F, Quinlan F, Cicak K, Aumentado J, Diddams S A and Teufel J D 2021 *Nature* **591** 575–579 URL https://doi.org/10.1038/s41586-021-03268-x

[19] Fox A G, Miller S E and Weiss M T 1955 *Bell Syst. Tech. J.* **34** 5–103 URL https://doi.org/10.1002/j.1538-7305.1955.tb03763.x

[20] Allen P J 1956 *IEEE Trans. Microw. Theory Techn.* **4** 223–227 URL https://doi.org/10.1109/TMTT.1956.1125066

[21] Freiser M 1968 *IEEE Trans. Magn.* **4** 152–161 URL https://doi.org/10.1109/TMAG.1968.1066210

[22] Kamal A, Clarke J and Devoret M H 2011 *Nat. Phys.* **7** 311–315 URL https://doi.org/10.1038/nphys1893

[23] Sliwa K M, Hatridge M, Narla A, Shankar S, Frunzio L, Schoelkopf R J and Devoret M H 2015 *Phys. Rev. X* **5**(4) 041020 URL https://doi.org/10.1103/PhysRevX.5.041020

[24] Estep N A, Sounas D L and Alù A 2016 *IEEE Trans. Microw. Theory Techn.* **64** 502–518 URL https://doi.org/10.1109/TMTT.2015.2511737

[25] Sounas D L and Alù A 2017 *Nat. Photonics* **11** 774–783 URL https://doi.org/10.1038/s41566-017-0051-x

[26] Kord A, Sounas D L and Alù A 2018 *IEEE Trans. Microw. Theory Techn.* **66** 911–926 URL https://doi.org/10.1109/TMTT.2017.2757470

[27] Kord A, Sounas D L and Alù A 2018 *IEEE Trans. Microw. Theory Techn.* **66** 2731–2745 URL https://doi.org/10.1109/TMTT.2018.2818152

[28] Del Bino L, Silver J M, Stebbings S L and Del'Haye P 2017 *Sci. Rep.* **7** 43142 URL https://doi.org/10.1038/srep43142

[29] Bino L D, Silver J M, Woodley M T M, Stebbings S L, Zhao X and Del'Haye P 2018 *Optica* **5** 279–282 URL https://doi.org/10.1364/OPTICA.5.000279

[30] Pan R K, Tang L and Xia K 2024 *Phys. Rev. A* **110**(4) 043505 URL https://doi.org/10.1103/PhysRevA.110.043505

[31] Xu X W and Li Y 2015 *Phys. Rev. A* **91**(5) 053854 URL https://doi.org/10.1103/PhysRevA.91.053854

[32] Shen Z, Zhang Y L, Chen Y, Zou C L, Xiao Y F, Zou X B, Sun F W, Guo G C and Dong C H 2016 *Nat. Photonics* **10** 657–661 URL https://doi.org/10.1038/nphoton.2016.161

[33] Ruesink F, Mathew J P, Miri M A, Alù A and Verhagen E 2018 *Nat. Commun.* **9** 1798 URL https://doi.org/10.1038/s41467-018-04202-y

[34] Shen Z, Zhang Y L, Chen Y, Sun F W, Zou X B, Guo G C, Zou C L and Dong C H 2018 *Nat. Commun.* **9** 1797 URL https://doi.org/10.1038/s41467-018-04187-8

[35] Xia K, Lu G, Lin G, Cheng Y, Niu Y, Gong S and Twamley J 2014 *Phys. Rev. A* **90**(4) 043802 URL https://doi.org/10.1103/PhysRevA.90.043802

[36] Scheucher M, Hilico A, Will E, Volz J and Rauschenbeutel A 2016 *Science* **354** 1577–1580 URL https://doi.org/10.1126/science.aaj2118

[37] Lodahl P, Mahmoodian S, Stobbe S, Rauschenbeutel A, Schneeweiss P, Volz J, Pichler H and Zoller P 2017 *Nature* **541** 473–480 URL https://doi.org/10.1038/nature21037

[38] Xia K, Nori F and Xiao M 2018 *Phys. Rev. Lett.* **121**(20) 203602 URL https://doi.org/10.1103/PhysRevLett.121.203602

[39] Li E Z, Ding D S, Yu Y C, Dong M X, Zeng L, Zhang W H, Ye Y H, Wu H Z, Zhu Z H, Gao W, Guo G C and Shi B S 2020 *Phys. Rev. Res.* **2**(3) 033517 URL https://doi.org/10.1103/PhysRevResearch.2.033517

[40] Zhang S, Lin G, Hu Y, Qi Y, Niu Y and Gong S 2020 *Phys. Rev. Appl.* **14**(2) 024032 URL https://doi.org/10.1103/PhysRevApplied.14.024032

[41] Tang L, Tang J s and Xia K 2022 *Adv. Quantum Technol.* **5** 2200014 URL https://doi.org/10.1002/qute.202200014

[42] Li J F, Wang Y F, Huang P S, Su K Y, Peng Y Q, Zhang S, Yan H and Zhu S L 2023 *Phys. Rev. Appl.* **20**(1) 014027 URL https://doi.org/10.1103/PhysRevApplied.20.014027

[43] Wang Y X, Wang C and Clerk A A 2023 *PRX Quantum* **4**(1) 010306 URL https://doi.org/10.1103/PRXQuantum.4.010306

[44] Tang L, Tang J, Chen M, Nori F, Xiao M and Xia K 2022 *Phys. Rev. Lett.* **128** 083604 URL https://doi.org/10.1103/PhysRevLett.128.083604

[45] Weedbrook C, Pirandola S, García-Patrón R, Cerf N J, Ralph T C, Shapiro J H and Lloyd S 2012 *Rev. Mod. Phys.* **84**(2) 621 URL https://link.aps.org/doi/10.1103/RevModPhys.84.621

[46] Grote H, Danzmann K, Dooley K L, Schnabel R, Slutsky J and Vahlbruch H 2013 *Phys. Rev. Lett.* **110** 181101 URL https://doi.org/10.1103/PhysRevLett.110.181101

[47] Liu K, Cai C, Li J, Ma L, Sun H and Gao J 2018 *Appl. Phys. Lett.* **113** 261103 ISSN 0003-6951 URL https://doi.org/10.1063/1.5066028

[48] Shi S, Wu Y, Liu X, Tian L, Li W, Wang Y and Zheng Y 2025 *Intell. Opto-Electron.* **1** 250002 URL https://doi.org/10.67704/ioe.2025.250002

[49] Li R, Jiao N, An B, Wang Y, Shi S, Tian L, Li W and Zheng Y 2026 *Optica* **13** 297–302 URL https://doi.org/10.1364/OPTICA.573701

[50] Yao W, Shi S, Lu B, Zheng L A, Zhang X, Zhao D, Li W, Chen L, Tian L, Wang Y and Zheng Y 2026 *Photon. Res.* **14** 3111–3119 URL https://doi.org/10.1364/PRJ.599557

[51] Kashiwazaki T, Takanashi N, Yamashima T, Kazama T, Enbutsu K, Kasahara R, Umeki T and Furusawa A 2020 *APL Photonics* **5** 036104 URL https://doi.org/10.1063/1.5142437

[52] Gao L, Zheng L a, Lu B, Shi S, Tian L and Zheng Y 2024 *Light Sci. Appl.* **13** 294 URL https://doi.org/10.1038/s41377-024-01606-y

[53] Lü X Y, Wu Y, Johansson J R, Jing H, Zhang J and Nori F 2015 *Phys. Rev. Lett.* **114**(9) 093602 URL https://doi.org/10.1103/PhysRevLett.114.093602

[54] Qin W, Miranowicz A, Li P B, Lü X Y, You J Q and Nori F 2018 *Phys. Rev. Lett.* **120**(9) 093601 URL https://doi.org/10.1103/PhysRevLett.120.093601

[55] Qin W, Macrì V, Miranowicz A, Savasta S and Nori F 2019 *Phys. Rev. A* **100**(6) 062501 URL https://doi.org/10.1103/PhysRevA.100.062501

[56] Burd S C, Srinivas R, Knaack H M, Ge W, Wilson A C, Wineland D J, Leibfried D, Bollinger J J, Allcock D T C and Slichter D H 2021 *Nat. Phys.* 898 URL https://doi.org/10.1038/s41567-021-01237-9

[57] Gardiner C W and Collett M J 1985 *Phys. Rev. A* **31**(6) 3761–3774 URL https://doi.org/10.1103/PhysRevA.31.3761

[58] Tang L, Tang J, Zhang W, Lu G, Zhang H, Zhang Y, Xia K and Xiao M 2019 *Phys. Rev. A* **99**(4) 043833 URL https://doi.org/10.1103/PhysRevA.99.043833

[59] Kutsaev S V, Krasnok A, Romanenko S N, Smirnov A Y, Taletski K and Yakovlev V P 2021 *Adv. Photonics Res.* **2** 2000104 URL https://doi.org/10.1002/adpr.202000104

[60] Zhang M, Wang C, Cheng R, Shams-Ansari A and Lončar M 2017 *Optica* **4**(12) 1536–1537 URL https://doi.org/10.1364/OPTICA.4.001536

[61] Desiatov B, Shams-Ansari A, Zhang M, Wang C and Lončar M 2019 *Optica* **6**(3) 380–384 URL https://doi.org/10.1364/OPTICA.6.000380

[62] Song W H, Guo D J, Yang R, Duan J C, Gu Z S, Tang J, Ye Z, Tian X H, Jia K, Yan Z, Yin Z, Gong Y X, Xie Z, Wang Z and Zhu S N 2025 *Chin. Phys. B* **34** 084205 URL https://doi.org/10.1088/1674-1056/adee8b

[63] Lu J, Li M, Zou C L, Sayem A A and Tang H X 2020 *Optica* **7**(12) 1654–1659 URL https://doi.org/10.1364/OPTICA.403931

[64] Tian Z, Zhang P and Chen X W 2021 *Phys. Rev. Appl.* **15**(5) 054043 URL https://doi.org/10.1103/PhysRevApplied.15.054043

[65] Jia X, Zhai C, Zhu X, You C, Cao Y, Zhang X, Zheng Y, Fu Z, Mao J, Dai T, Chang L, Su X, Gong Q and Wang J 2025 *Nature* **639** 329–336 URL https://doi.org/10.1038/s41586-025-08602-1

[66] Lu L, Xia L, Chen Z, Chen L, Yu T, Tao T, Ma W, Pan Y, Cai X, Lu Y, Zhu S and Ma X S 2020 *npj Quantum Inf.* **6** 30 URL https://doi.org/10.1038/s41534-020-0260-x

[67] Zheng X, Jing X, Liu C, Li Y, He R, Xia L, Wang F, Kong Y, Chen T, Lu L, Dai J and Niu B 2026 *arXiv: 2601.08289* URL https://arxiv.org/abs/2601.08289